https://doi.org/10.3847/2041-8213/ab1aab

On the Time–Frequency Downward Drifting of Repeating Fast Radio Bursts

Weiyang Wang[1,2,3] , Bing Zhang[4] , Xuelei Chen[1,2,5], and Renxin Xu[3,6,7]

[1] Key Laboratory for Computational Astrophysics, National Astronomical Observatories, Chinese Academy of Sciences, 20A Datun Road, Beijing 100101, People's Republic of China; wywang@bao.ac.cn

[2] University of Chinese Academy of Sciences, Beijing 100049, People's Republic of China

[3] School of Physics and State Key Laboratory of Nuclear Physics and Technology, Peking University, Beijing 100871, People's Republic of China

[4] Department of Physics and Astronomy, University of Nevada, Las Vegas, NV 89154, USA; zhang@physics.unlv.edu

[5] Center for High Energy Physics, Peking University, Beijing 100871, People's Republic of China

[6] Kavli Institute for Astronomy and Astrophysics, Peking University, Beijing 100871, People's Republic of China

[7] Department of Astronomy, School of Physics, Peking University, Beijing 100871, People's Republic of China

Abstract

The newly discovered second repeating fast radio burst (FRB) source, FRB 180814.J0422+73, was reported to exhibit a time–frequency downward drifting pattern, which is also seen in the first repeater FRB 121102. We propose a generic geometrical model to account for the observed downward drifting of sub-pulse frequency, within the framework of coherent curvature radiation by bunches of electron–positron pairs in the magnetosphere of a neutron star (NS). A sudden trigger event excites these coherent bunches of charged particles, which stream outward along open field lines. As the field lines sweep across the line of sight, the bunches seen later travel farther into the less-curved part of the magnetic field lines, thus emitting at lower frequencies. We use this model to explain the time–frequency downward drifting in two FRB generation scenarios, the transient pulsar-like sparking from the inner gap region of a slowly rotating NS, and the externally triggered magnetosphere reconfiguration known as the "cosmic comb."

Key words: pulsars: general – radiation mechanisms: non-thermal – radio continuum: general – stars: neutron

1. Introduction

Fast radio bursts (FRBs) are mysterious millisecond-duration astronomical radio transients with large dispersion measures in excess of the Galactic value (DM $\gtrsim$ 200 pc cm^{-3}, Lorimer et al. 2007; Keane et al. 2012; Thornton et al. 2013; Kulkarni et al. 2014; Petroff et al. 2015, 2016; Chatterjee et al. 2017). The cosmological origin of FRBs was established after FRB 121102, the first repeating source (Spitler et al. 2016), was localized in a star-forming dwarf galaxy at $z = 0.193$ with an associated persistent radio source (Bassa et al. 2017; Chatterjee et al. 2017; Marcote et al. 2017; Tendulkar et al. 2017) and an extreme magneto-ionic environment (Michilli et al. 2018).

Recently, the CHIME/FRB Collaboration et al. (2019) reported the discovery of the second repeating FRB source, FRB 180814.J0422+73. Very intriguingly, both FRB 121102 and FRB 180814.J0422+73 showed an interesting sub-pulse time–frequency downward drifting pattern in at least some of their bursts. For these bursts, each burst have several sub-pulses, with the later-arrival sub-pulses having lower frequencies (Hessels et al. 2018; CHIME/FRB Collaboration et al. 2019). This time–frequency structure is reminiscent to the Type III solar bursts and the decametric radiation from Jupiter (Bastian et al. 1998; Treumann 2006). However, it is unclear whether the same mechanism is at work, as the FRBs are at cosmological distances and have extremely high brightness temperatures. Plasma lensing may cause a sub-pulse drift, but both upward and downward drifts are expected (Cordes et al. 2017). In contrast, only the downward drifting is seen in the repeating FRBs. A mechanism intrinsic to the FRB source is most likely the origin of the drift. One such mechanism has been proposed in the framework of magnetar-wind-driven external shock synchrotron masers (Metzger et al. 2019). However, in this model it is not clear why such down drifting does not occur in consecutive individual bursts.

Here we propose an alternative model by invoking coherent curvature radiation in a neutron star (NS) magnetosphere. Sub-pulse drifting is a well-known phenomenon in radio pulsars (Rankin 1990), which can be interpreted as $E \times B$ drift in the inner gap where the particles are accelerated from the polar cap region (Ruderman & Sutherland 1975). Curvature radiation from charge bunches from pulsar magnetospheres has been invoked to interpret FRB coherent radio emission by several authors (e.g., Katz 2014; Kumar et al. 2017; Lu & Kumar 2018; Yang & Zhang 2018). In this Letter, we propose a generic geometrical mechanism to account for the observed time–frequency downward drifting from the two repeating FRBs. The model is described in Section 2, and its applications in two specific scenarios are discussed in Section 3.

2. Geometric Model

We consider a generic model of coherent curvature radiation by bunches of charged particles in a NS magnetosphere. The specific geometry does not matter, as long as the bunches are generated abruptly and stream outward along open magnetic field lines. The field lines sweep across the line of sight (LOS) as the magnetosphere rotates. The observer sees emission from several bunches of neighboring magnetic field lines. Assuming that the Lorentz factors of the bunches are the same from each other and do not evolve significantly as they stream along the field lines, the bunches observed earlier emit curvature radiation in the more-curved part of the field lines, and therefore have higher frequencies. In contrast, the bunches observed later emit in the less-curved part of the field lines with lower frequencies.

Figure 1 shows a schematic plot of one version of such field lines, where the "sparks" are produced from the inner magnetosphere of the open field lines of an NS. The sparks are produced at a low height due to a sudden release of energy,
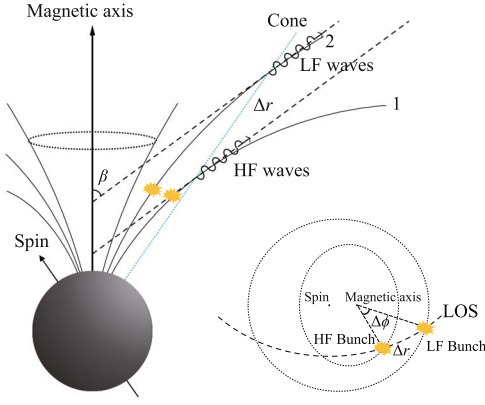
Figure 1. Schematic diagram of the first scenario, with sparks originating from the polar gap region. The HF waves are emitted from lower altitudes than the LF waves. The left panel shows the initial configuration when the two sparks are produced around the same location. The dashed lines show the LOS. The second spark sweeps the LOS at a higher altitude. The right panel shows the sky map of two sparks. These two sparks sweep the LOS at different heights at different times.

e.g., by magnetic reconnection or crust cracking. Several bunches are released around the same time and continuously radiate along neighboring field lines. In the plot, two locations are marked for the sub-pulses of high frequency (HF) and low frequency (LF). The two locations for the two sub-pulse emission are different in radius (Δr) and in azimuthal angle ($\Delta\phi$).

The emission frequency of curvature radiation reads $\nu = (3/4\pi)\gamma^3(c/\rho)$, where ρ is the curvature radius, and c is speed of light. Assuming a constant Lorentz factor γ of the charges, the change in the typical curvature radiation frequency is given by

$$\Delta\nu = -\frac{3c\gamma^3\Delta\rho}{4\pi\rho^2} = -\nu\frac{\Delta\rho}{\rho}, \tag{1}$$

where $\Delta\rho$ is the change in the curvature radius between the two emitting points. Observationally, $\Delta\nu/\nu$ is of the order of 0.1 (Hessels et al. 2018; CHIME/FRB Collaboration et al. 2019), so we can infer $\Delta\rho/\rho \sim 0.1$ for a constant γ.

If the bunch scale is smaller than the half-wavelength (~ 10 cm, for 1 GHz), the phase of emission radiated by each particle in the bunch would be approximately the same, so coherent radio emission is produced (Melrose 2017; Kumar et al. 2017; Yang & Zhang 2018). The GHz curvature radiation timescale for such a bunch is 1 ns, which is much shorter than that of the observed pulse duration ~ 1 ms, so there must be more than one bunch sweeping cross the LOS (Yang & Zhang 2018). Such intense sparks likely happen in an environment with an abrupt release of a huge amount of energy to produce FRBs.

Most generically, the observed time delay of LF wave with respect to the HF wave can be written as

$$\Delta t = \Delta t_\phi + \Delta t_r, \tag{2}$$

where Δt_ϕ is the interval between the two emission beams sweeping across the LOS, and Δt_r is the delay of emission in the radial direction for the two sparks, i.e., the retardation delay

(see Figure 1). One can generally write

$$\Delta t_\phi = \frac{\Delta r_\perp}{v}, \tag{3}$$

where $\Delta r_\perp$ is the projected horizontal distance between the HF-emitting region and the LF-emitting region, and v is the projected speed of the sweeping beam. As the two sparks are generated simultaneously but the observed emissions from the two sparks are emitted at different epochs, the delay of receiving the two signals due to the retardation delay can be estimated as

$$\Delta t_r = \frac{\Delta r}{v_e} - \frac{\Delta r}{c} \approx \frac{\Delta r}{2\gamma_e^2 c}, \tag{4}$$

where $v_e \sim c$ is the velocity of the electrons (or pairs) in the bunches, and γ_e is its corresponding Lorentz factor.

3. Applications

In this section, we apply this generic geometrical model to two specific scenarios of FRB production. The first scenario is a transient pulsar sparking model with the FRB originating from the pulsar inner gap region. The magnetic field configuration in this scenario may be approximated as a simple dipole. The second scenario is the cosmic comb model (Zhang 2017, 2018). The sparks are suddenly generated upon the interaction between the external plasma stream and the pulsar magnetosphere, which flow along the open field lines in the sheath. The field line configuration is not dipolar, but is more stretched. In both cases, the sparks propagate from high-curvature regions to low-curvature regions, leading to frequency downward drifting. We now discuss these two scenarios in turn.

3.1. Polar Gap Sparking

For the first scenario, we consider an FRB generated from the polar gap region of a pulsar. This could be related to a young regular field pulsar (e.g., Connor et al. 2016; Cordes & Wasserman 2016) or a young magnetar with the emission coming from the inner magnetosphere (Kumar et al. 2017).

We consider a scenario similar to the polar gap sparking of the regular pulsars (Ruderman & Sutherland 1975). However, instead of invoking regular, continuous sparks, we envisage a sudden, violent sparking process from the surface, possibly triggered by an abrupt crust cracking that leads to an abrupt magnetic field dissipation. A significant deviation from the regular magnetic field configuration is triggered, which leads to coherent curvature radiation by bunches of charged particles in a lotus of field lines (Yang & Zhang 2018). The perturbation propagates along the field lines outward, leading to multiple sparks emitting in adjacent field line bundles traveling with a similar Lorentz factor.

Consider that the polar gap of the pulsar is enclosed within the last open field lines with a polar angle $\theta_p = 0.1(P/10\ \mathrm{ms})^{-1/2}$, where P is the period of the pulsar. For a dipole magnetic field, a magnetic field line can be described as

$$u = \frac{R\sin^2\theta}{r}, \tag{5}$$

where R is the radius of the NS surface, and u is a dimensionless constant. The curvature radius of the field line

is (for $\theta \lesssim 0.5$)

$$\rho = \frac{r(1 + 3\cos^2\theta)^{3/2}}{3\sin\theta(1 + \cos^2\theta)} \approx \frac{4r}{3\sin\theta}. \qquad (6)$$

For $\gamma_e = 300$, the curvature radius is estimated to be $\rho \simeq 1.9 \times 10^8$ cm to produce $\sim$GHz curvature radiation.

For a dipolar geometry, the time for the line to sweep a phase $\Delta\phi$ is given by

$$\Delta t_\phi = \frac{P\sin\beta\Delta\phi}{2\pi\sin(\alpha + \beta)}, \qquad (7)$$

where P is the period of the pulsar, α is the magnetic inclination angle, and β is the impact angle of the LOS with respect to the magnetic axis. In this scenario, Δt_ϕ only depends on the geometry of the pulsar. As an example, we assume $\Delta r = 0.01\rho$. From Equation (4), one can estimate the retardation time delay to be $\Delta t_r \simeq 10$ ns, which is much smaller than the observed interval times between sub-pulses ~ 0.1–10 ms (Hessels et al. 2018; CHIME/FRB Collaboration et al. 2019). Hence, the time delay of LF waves with respect to the HF waves is mainly given by the sweeping delay Δt_ϕ.

Combining Equations (3), (5), and (6), one gets

$$\dot{\nu} = A_g\nu = \frac{2\pi\sin(\alpha + \beta)\Delta u}{uP\sin\beta\Delta\phi}\nu. \qquad (8)$$

According to Equation (8), when the geometrical condition of $\Delta\phi/\Delta u \simeq -2\pi u^{-1}(P/10 \text{ ms})^{-1}[\sin(\alpha + \beta)/\sin\beta]$ is satisfied, the drifting rate is very similar to what is observed in FRB 121102 (Hessels et al. 2018). If $\Delta t_\phi \ll |1/A_g|$, the central frequency decreases linearly with time. This scenario matches the observations of FRB 180814.J0422+73 well (CHIME/FRB Collaboration et al. 2019).

At the same height, electrons are in different trajectories with essentially the same curvature radius. Because different field lines have slightly different curvatures, the condition of coherence is that the bunch opening angle $\Delta\phi_b$ should be smaller than $1/\gamma_e$ (Yang & Zhang 2018). Defining $\nu_\phi = 12c/(\pi\rho\Delta\phi_b^3)$, the condition $\nu < \nu_\phi$ can be translated to $\Delta\phi_b < 1/\gamma_e$. Observationally, the sub-pulse interval time is of the order of milliseconds (Hessels et al. 2018; CHIME/FRB Collaboration et al. 2019), $\Delta t \sim (1 \text{ ms})\Delta t_{ms}$. The condition $\Delta\phi < 1/\gamma_e$ can be satisfied if the pulsar period satisfy $P > \gamma_e\Delta t = 0.3 \text{ s}(\gamma_e/300)\Delta t_{ms}$.

3.2. Cosmic Comb

In the cosmic comb model (Zhang 2017, 2018) a plasma stream from a nearby source interacts with a pulsar. Similar to solar wind interacting with the earth magnetosphere, the external stream would re-structure the magnetosphere of the pulsar, forming an elongated magnetosphere surrounded by a sheath. The FRB is seen when the sheath plasma sweeps the LOS. For GHz radio waves, one requires $\gamma_e \sim 10^3$ for the curvature radius $\rho \sim 10^{10}$ cm that matches the light cylinder radius $R_{LC} = 4.8 \times 10^9$ cm $(P/1 \text{ s})$. As this is an abrupt process caused by the ram pressure overcoming the magnetic pressure, the field line is significantly distorted from the dipolar form.

We envisage that the sudden distortion of the magnetosphere would drive significant electric density fluctuation with respect to the original Goldreich–Julian value, forming sparks or bunches of charged particles in a lotus of field lines around the same time. These sparks from different field lines stream outward and sweep the LOS at different times. Figure 2 shows a schematic view of this process for three different epochs when three sparks sweep the LOS. One can see that the spark observed by the observer earlier originates at a lower altitude and hence has a higher frequency. As different field lines sweep across the LOS, emission with progressively decreasing frequency is observed due to the progressively larger curvature radius along these field lines.

Again the retardation delay time $\Delta t_r \sim 1.7 \times 10^{-5} \text{ s} \Delta r_{12}\gamma_{e,3}^{-2} \ll \Delta t$ (the convention $Q_n = Q/10^n$ in cgs units is adopted). Therefore, the observed delay time is mostly defined by the sweeping delay, which reads

$$\Delta t_\phi \simeq \frac{\Delta R_s}{v_s\gamma_e} \approx (3 \text{ ms})\Delta R_{s,10} v_{s,-1}^{-1} \gamma_{e,3}^{-1}, \qquad (9)$$

where ΔR_s is the size of the sheath, $r_\perp = R_s/\gamma_e$ is the projected distance in the sky when the emission beam is observed, and $v_s \simeq 0.1c \, v_{s,-1}$ is the velocity of the stream that combs the magnetosphere. This is consistent with the observed millisecond interval time of the sub-pulses. Equation (9) has properties similar to Equation (7).

Combining Equations (1), (3), and (9), one can obtain

$$\dot{\nu} = A_c\nu = -\frac{v_s\gamma_e\Delta\rho}{\rho\Delta R_s}\nu \qquad (10)$$

for the cosmic comb model. One can estimate that $\Delta\rho/\Delta R_s \simeq 0.3\rho_{10}\gamma_{e,3}^{-1}$. The frequency drifting rates would decrease linearly with ν, which is consistent with the observations of FRB 121102. The drifting rate would be a constant when $\Delta t \ll |1/A_c|$ for each multi-sub-pulse sequence. In such a situation, the result matches the observations of FRB 180814.J0422+73.

3.3. Drifting Rates

Equations (8) and (10) show that both models share the similar feature of frequency down-drifting. In Figure 3, we show the simulated sub-pulse central frequency drift as a function of the arrival time for the parameter $A_g = A_c = -0.01 \text{ ms}^{-1}$. We fix $\Delta t = 1$ ms but allow the central frequency to vary. From up to down, different curves (with different colors) stand for different central frequencies: 6.5 GHz (red diamonds), 2.2 GHz (green squares), 1.4 GHz (blue triangles), and 400 MHz (black dots). These results are generally consistent with the observations of the two FRB repeaters (Hessels et al. 2018; CHIME/FRB Collaboration et al. 2019).

3.4. Particle Cooling and Acceleration

In the above discussion, we have assumed a constant γ for both models. For typical FRB parameters, both models involve rapid cooling of the emitting particles (the cooling rate increases by a factor of N_e for coherent emission by bunches, where N_e is the

(a)

(b)

(c)
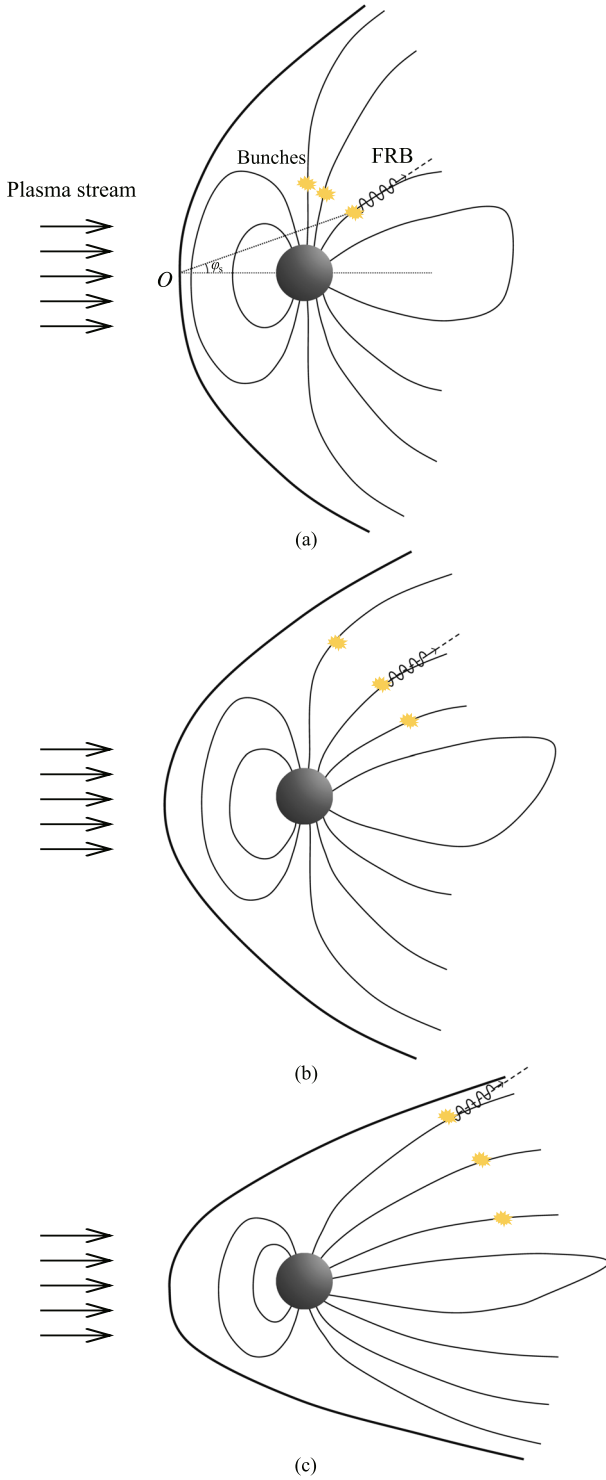
Figure 2. Schematic diagram of the second scenario in the cosmic comb model. The sparks are produced in the distorted sheath region, which stream outward along the field lines. For the illustrative purpose, the separations between the field lines are stretched. Sparks from different field lines sweep the LOS at different times when the sparks reach different heights. The spark observed at a later epoch emits at a less-curved part of field line and thus has a lower frequency. A burst with three sub-pulses is shown for illustration, with three epochs: (a) the inner spark emission beams toward the LOS; (b) an intermediate spark emission beams toward the LOS; (c) the outer spark beams toward the LOS.

number of net electrons in the bunch) and therefore require continuous acceleration of the bunched particles. Very generally, the cooling timescale of curvature radiation in the observer's rest
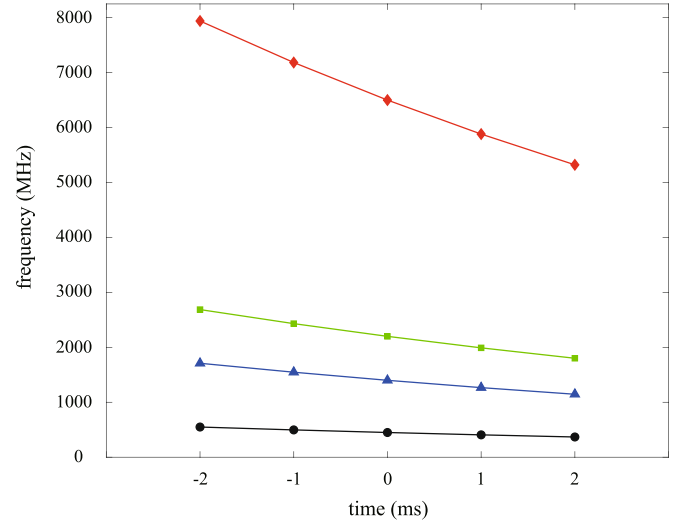
Figure 3. Simulated sub-burst central frequency as a function of the arrival time. We assume $A_g = A_c = -0.01\ \mathrm{ms^{-1}}$. The sub-burst sequences have different central frequencies with the same interval time $\Delta t = 1$ ms: 6.5 GHz (red diamonds), 2.2 GHz (green squares), 1.4 GHz (blue triangles), and 400 MHz (black dots).

frame can be written as (Kumar et al. 2017)

$$t_{\rm cool} \sim \frac{27 m_e c^3 \gamma_e^3}{16 \pi^2 e^2 \nu^2 N_e} \sim 1.8 \times 10^{-13} \gamma_{e,2}^3 \nu_9^{-2} (N_{e,23})^{-1}\ \mathrm{s}. \quad (11)$$

Therefore, to sustain a constant Lorentz factor within a lab-frame time duration of γ^2/ν, one requires that there exists an electric field parallel $E_\parallel$ to the B-field that can accelerate electrons, which is given by

$$E_\parallel \simeq \frac{\gamma_e m_e c}{(e t_{\rm cool})} \sim 3.1 \times 10^7 \nu_9^2 N_{e,\,23} \gamma_{e,\,2}^{-2}\ \mathrm{esu}. \quad (12)$$

For the scenario of polar gap sparking, the electron number may be described by (e.g., Kumar et al. 2017)

$$N_e \simeq \frac{\mu B c^2 \gamma_e^3}{\nu^3 e P} = 1.9 \times 10^{24} \mu B_{14} \gamma_{e,2}^3 P_{-1}^{-1} \nu_9^{-3}, \quad (13)$$

where μ is the normalized fluctuation of electrons deviated from the Goldreich–Julian density. The required electric field is calculated as $E_\parallel \sim 5.9 \times 10^8 \mu B_{14} P_{-1}^{-1} \gamma_{e,\,2} \nu_9^{-1}$ esu. One possible mechanism to create such an electric field is the sudden magnetic reconnection in the magnetosphere.

Within the cosmic comb model, the electron number is given by (Yang & Zhang 2018)

$$N_e \simeq \frac{\mu \eta B R^3 L}{2 \pi e R_{\rm LC}^2} = 3.3 \times 10^{19} \mu \eta B_{12} R_6^3 L_1 (R_{\rm LC,10})^{-2}, \quad (14)$$

where $\eta R_{\rm LC}^2$ is the cross section of the bunch in nearly parallel field lines in the combed magnetosphere, and $L \sim \lambda$ is the thickness of the bunch, which is comparable to the wavelength λ of the emission. The required electric field for this model is then $E_\parallel \sim 100 \mu \eta B_{12} \nu_9^2 R_6^3 L_1 (R_{\rm LC,10})^{-2} \gamma_{e,3}^{-2}$ esu. The strong ram pressure of the stream likely would reconfigure the magnetic field suddenly to provide the required electric field to accelerate electrons.

4. Summary and Discussion

We proposed a generic geometrical mechanism to explain the frequency downward drifting within the framework of coherent curvature radiation in the magnetosphere of an NS. As long as the sparks or bunches of charged particles are produced abruptly from the inner magnetosphere of an NS, and stream outward along the open field lines, a spark observed at an earlier time was always emitted in a more-curved part of field line, hence at a higher frequency than one observed later, which had traveled to a less-curved part of the field line, hence emitting at a lower frequency. As a result, the frequency-time downward drifting is a natural consequence of coherent curvature radiation. We argue that this may be considered an evidence of the fact that the FRB radio emission originates from a pulsar magnetosphere. We apply this generic geometrical model to explain the frequency drifting within two scenarios: (a) the transient pulsar-like sparking from the inner gap of a slowly rotating NS; and (b) the cosmic comb. Both models can reproduce the observations with reasonable parameters.

For the transient sparking scenario of isolated NSs, the condition is that the NS rotation period cannot be too short. This actually poses some constraints on the spindown-powered models. For the young pulsar model in supernova remnants (e.g., Connor et al. 2016; Cordes & Wasserman 2016), a slow rotator would give a spindown luminosity that is significantly below the FRB luminosity, making it difficult to power FRBs. For the magnetically powered (magnetar) models, the energy budget issue is less demanding (Kumar et al. 2017). However, the requirement of having emission from the open field line region poses some constraints on some versions of the model (e.g., Lu et al. 2019). Alternatively, the FRBs may be triggered internally by, say, starquakes (Wang et al. 2018). In this case, the FRBs should be accompanied by global oscillations and glitches. The cosmic comb model (Zhang 2017, 2018) invokes the outer magnetosphere of an NS as the site of FRB emission. It can also naturally produces sub-pulse down-drifting, with the ultimate energy coming from the kinetic energy of the external stream.

In our geometric model, the sparks are modeled as isolated bunches for simplicity. In reality, the outflow is likely continuous in adjacent field lines but with density fluctuations. This would give rise to continuous emission with distinct peaks, as the observations show. In contrast to the continuous sparking in the polar cap region of normal pulsars, our model invokes a sudden, violent sparking process. The FRB flow is likely abrupt and non-uniform across different field lines, which is likely the case in both scenarios discussed in this Letter.

ORCID iDs

Weiyang Wang https://orcid.org/0000-0001-9036-8543
Bing Zhang https://orcid.org/0000-0002-9725-2524

References

Bassa, C. G., Tendulkar, S. P., Adams, E. A. K., et al. 2017, ApJL, 843, L8
Bastian, T. S., Benz, A. O., & Gary, D. E. 1998, ARA&A, 36, 131
Chatterjee, S., Law, C. J., Wharton, R. S., et al. 2017, Natur, 541, 58
CHIME/FRB Collaboration, Amiri, M., et al. 2019, Natur, 566, 235
Connor, L., Sievers, J., & Pen, U.-L. 2016, MNRAS, 458, L19
Cordes, J. M., & Wasserman, I. 2016, MNRAS, 457, 232
Cordes, J. M., Wasserman, I., Hessels, J. W. T., et al. 2017, ApJ, 842, 35
Hessels, J. W. T., Spitler, L. G., Seymour, A. D., et al. 2018, arXiv:1811.10748
Katz, J. I. 2014, PhRvD, 89, 103009
Keane, E. F., Stappers, B. W., Kramer, M., & Lyne, A. G. 2012, MNRAS, 425, L71
Kulkarni, S. R., Ofek, E. O., Neill, J. D., Zheng, Z., & Juric, M. 2014, ApJ, 797, 70
Kumar, P., Lu, W., & Bhattacharya, M. 2017, MNRAS, 468, 2726
Lorimer, D. R., Bailes, M., McLaughlin, M. A., Narkevic, D. J., & Crawford, F. 2007, Sci, 318, 777
Lu, W., & Kumar, P. 2018, MNRAS, 477, 2470
Lu, W., Kumar, P., & Narayan, R. 2019, MNRAS, 483, 359
Marcote, B., Paragi, Z., Hessels, J. W. T., et al. 2017, ApJL, 834, L8
Melrose, D. B. 2017, RvMPP, 1, 5
Metzger, B. D., Margalit, B., & Sironi, L. 2019, MNRAS, 485, 4091
Michilli, D., Seymour, A., Hessels, J. W. T., et al. 2018, Natur, 553, 182
Petroff, E., Barr, E. D., Jameson, A., et al. 2016, PASA, 33, e045
Petroff, E., Johnston, S., Keane, E. F., et al. 2015, MNRAS, 454, 457
Rankin, J. M. 1990, ApJ, 352, 247
Ruderman, M. A., & Sutherland, P. G. 1975, ApJ, 196, 51
Spitler, L. G., Scholz, P., Hessels, J. W. T., et al. 2016, Natur, 531, 202
Tendulkar, S. P., Bassa, C. G., Cordes, J. M., et al. 2017, ApJL, 834, L7
Thornton, D., Stappers, B., Bailes, M., et al. 2013, Sci, 341, 53
Treumann, R. A. 2006, A&ARv, 13, 229
Wang, W., Luo, R., Yue, H., et al. 2018, ApJ, 852, 140
Yang, Y.-P., & Zhang, B. 2018, ApJ, 868, 31
Zhang, B. 2017, ApJL, 836, L32
Zhang, B. 2018, ApJL, 854, L21